An Algorithm for Accurate Needle Orientation

Yifan Yang[1], Amr Ahmed[2], Shigang Yue[2], Xiang Xie[*1], Hong Chen[1], and Zhihua Wang[1]

***Abstract*— For the early diagnosis and treatment, a needle insertion for biopsy and treatment is a common and important means. To solve the low accuracy and high probability of repeat surgery in traditional surgical procedures, a computer-assisted system is an effective solution. In such a system, how to acquire the accurate orientation of the surgical needle is one of the most important factors. This paper proposes a "Center Point Method" for needle axis extraction with high accuracy. The method makes full use of edge points from two sides of the needle in image and creates center points through which an accurate axis is extracted. Experiments show that the proposed method improves needle orientation accuracy by approximately 70% compared to related work in binocular stereovision system.**

I. Introduction

In recent several years, due to its high accuracy, surgical navigation has become more and more popular in computer assisted surgery. In traditional surgical procedures for the biopsy and treatment of the tumor inside the body, it is critical to hit the tumor target through a surgical needle from outside body. In general, surgeons firstly locate the tumor target inside the body through medical images (CT for example). Secondly, according to these images, surgeons design the entry point on patient's body as well as the orientation of surgical needle. Thirdly, the surgeon holds the needle by hand to approach the entry point and revise the needle orientation to the designed one depending on his/her own experience. Finally, the surgeon punctures the needle into the patient's body. To verify whether the needle reach the tumor target or not, the patient will be scanned again to get new CT images. After analyzing these new images, if the target was not reached, the surgeon will pull out the needle and repeat the process again. Obviously, there is a high risk to cause great harm to patients, if this process repeats several times. This includes possible damage to some crucial nearby organs, due to any errors/inaccuracy of needle orientation.

In order to overcome the shortcoming in traditional surgery, a computer-assisted system should be used. This system must provide a high accuracy of the needle position and orientation in real time to surgeon, instead of relying on their individual experience. A series of related studies about image-guide computer assisted surgery have been published in literatures. Those studies can be divided into two classes.

The first class is using infrared cameras to track the spheres mounted on the surgical instrument. Treepong et al. [1], Bootsma et al. [2] and Zheng et al. [3] use the Polaris® Vicra® optical to track the passive spheres that are attached to the biopsy needle. Yang et al. [4] introduced a near infrared optical tracking system to track a specific needle with three spheres. As mentioned in [1] and [4], before this tracking can work, the spatial relationship between needle and the spheres need to be calibrated firstly. During this calibration procedure, needle tip need to be fixed on an invariant position and the surgical tool is swayed manually. There are two problems in this calibration procedure. Firstly, for needle tip on an invariant position, needle tip must be sterilized after this calibration procedure. Secondly, it is hard to ensure the needle tip on an invariant position manually all the time. Hence, the accuracy of this calibration procedure is limited. The second class is using visible light cameras or medical imaging device to directly track surgical needle using certain image processing technique. For the detection of straight surgical needle in image, Hough Transform (HT in short) is a widely used technique. Nicolau et al. [5], Goffin et al. [6], Ayadi et al. [7], Hong et al. [8] and Garcia-Morales et al. [9] utilized Hough Transform (HT) for needle recognition. Zhou et al.[10] used Improved Hough Transform in 3D Ultrasound Images. Although Hough Transform is noise immunity, fault tolerance and robustness, directly using Hough Transform detected lines (HT lines) to calculate needle orientation is limited accurate, for multiple solutions of Hough Transform in detecting lines.

This paper proposes an improved algorithm called "Center Point Method" for needle axis extraction to solve the problem mentioned in the second class. The method, instead of directly using HT lines to compute needle axis, utilizes two sides of edge points restored from HT lines and create center points through which an axis is extraction for higher accuracy. The paper is organized as follows: Section Ⅱ details our proposed center point method for needle axis extraction. Section Ⅲ presents the experimental results. Finally, the paper is concluded in section Ⅳ.

II. The Proposed Center Point Method

Before illustrating the proposed center point method, the principle of 3D orientation calculation of surgical needle is introduced to show how to calculate 3D orientation through needle axes from left and right image in binocular stereovision system as shown in Fig. 1.

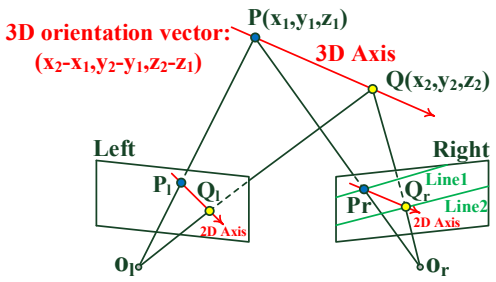

Fig. 1. The principle of 3D orientation calculation.

*This research was supported by Science and Technology Project of Shenzhen (JCYJ20150331151358146), Independent research project of Tsinghua University (NO.20131089223), the National Natural Science Foundation of China (grant NO.61373073) and EU FP7 IRSES projects, via EYE2E (269118) and LIVCODE (295151).

[1]Institute of Microelectronics, Tsinghua University, Beijing 100084, China.(corresponding author: Xiang Xie; e-mail: xiexiang@tsinghua.edu.cn)

[2]School of Computer Science, University of Lincoln, UK

Under the assumption that the model of camera is pinhole, the principle of binocular stereo vision system [11] to determine needle orientation is shown in Fig. 1. The red line in left/right image plane is the extracted 2D needle axis. P_l and Q_l are the two points selected on axis in left image plane. In right image plane, Line1 and Line2 are the epipolar lines. Line1 = Plane $O_lP_lO_r$ ∩ Right image plane while Line2 = Plane $O_lQ_lO_r$ ∩ Right image plane. O_l and O_r are the optical center of left and right cameras respectively. The matching points of P_l and Q_l are P_r and Q_r, which are determined by the intersections of axis and Line1/Line2 respectively. Through these two group of matching points and the intrinsic and extrinsic parameters of two cameras, the coordinates of P and Q in 3D space are computed. Finally, the orientation vector in 3D space is computed by subtracting these two coordinates. Assume the needle is downward.

According to the above principle, axis extraction in left/right image plane is a vital step for 3D orientation calculation and its accuracy will influence the final 3D orientation accuracy. Hence, to improve the orientation accuracy, an accurate 2D axis extraction algorithm is proposed.

This algorithm is combined by two parts. One is needle edge points recovery based on HT lines, the other is axis extraction based on needle edge points.

A. Needle Edge Points Recovery Based on HT lines

The procedure of surgical needle edge points recovery is shown in Fig. 2. It is noted that the background of the needle is pure in this research. It is reasonable because the acquisition of the surgical needle orientation happens only in the system calibration stage of the surgical navigation application.

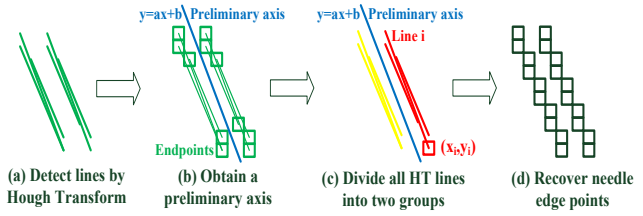

Fig. 2. Edge points recovery.

Step 1: Utilizing edge detection and Hough Transform to detect lines and obtain HT line segments (see in Fig. 2a).

Step 2: In Fig. 2b, the preliminary axis is obtained by fitting all HT lines' endpoints (illustrated in Fig. 2b as squares) using the least squares method. This preliminary axis tends to parallel with needle borders (not other orientation, for example, a line that is perpendicular to the axis in Fig. 2b), because the needle is narrow in images. The purpose to obtain preliminary axis is to divide all the HT lines into two sides.

Step 3: According to the preliminary axis, all HT lines in Fig. 2a are divided into two groups (yellow and red group in Fig. 2c) which are corresponding to two sides of needle edges. The method to divide HT lines into these two groups is as follows. We compare each HT line segment to the preliminary axis one by one and judge which group the HT line belongs to. Assume the function of the preliminary axis is $y = ax + b$ and the coordinate of the ith line's endpoint (in Fig. 2c) is (x_i, y_i). We substitute (x_i, y_i) into the judgment function:

$$f = y_i - ax_i - b \quad (1)$$

If f<0, we attribute this HT line (ith line) to group1, else attribute to group2. Hence, according to this judgment, all the HT lines are divided into two groups which correspond to different sides of the needle.

Step 4: From these two groups of HT lines in Fig. 2c, each side of needle edge points (Fig. 2d) are recovered by the corresponding HT lines group.

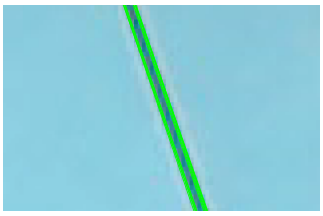

Fig. 3. Hough lines.

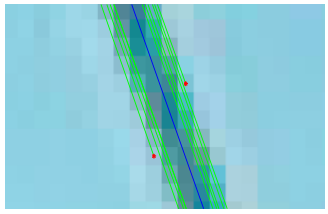

Fig. 4. Preliminary axis.

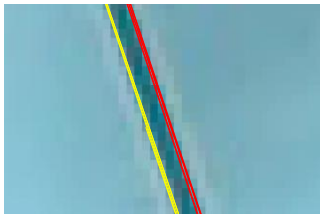

Fig. 5. Two groups of obtained lines.

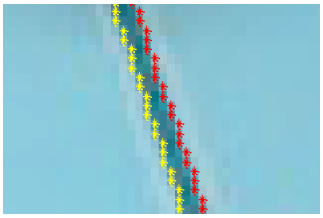

Fig. 6. Border points.

Fig. 3~6 displays the experiment results of the procedure. (1) Fig. 3 shows the detected HT lines (green lines) on needle borders in step 1. (2) Fig. 4 is the result in step 2. The red points are the endpoints of the HT lines and the blue line is the preliminary axis. (3) In Fig. 5, all the HT lines in Fig. 3 are divided into yellow and red group as described in step 3. (4) In Fig.6, the yellow points are recovered by all the HT lines in yellow group while the red points are recovered by all the HT lines in red group.

B. Axis Extraction Based on needle edge points

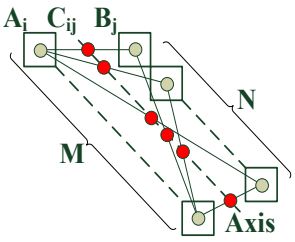

Fig. 7. Axis extraction algorithm.

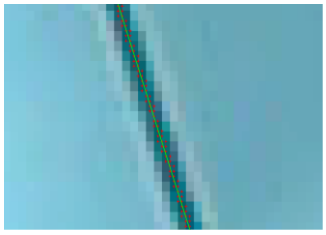

Fig. 8. Center points and extracted axis.

As shown in Fig. 7, the squares are the needle border pixels which are obtained from section Ⅱ-A.

A_i (i=1,2,…,M), B_j (j=1,2,…,N) represent the left and right border points respectively. C_{ij} is the midpoint (center points) of A_i and B_j. No matter what value of i and j are, C_{ij} must be the point on the needle axis if no error exists. An accurate needle axis is obtained by fitting C_{ij} using the least squares method. The number of the center points used to fitting the axis ranges from 2 to M×N. An experiment result is shown in Fig. 8 which displays a series of center points (red) created by edge points from Fig. 6 and the final fitting axis (green).

No matter what kind of methods, the needle border points are the original information. Therefore, needle axis extraction errors stem from border errors. In Fig. 7, assume the coordinate of A_i and B_j are $(x_{Ai}+\Delta x_{Ai}, y_{Ai}+\Delta y_{Ai})$ and $(x_{Bj}+\Delta x_{Bj}, y_{Bj}+\Delta y_{Bj})$ respectively. x_{Ai}, y_{Ai}, x_{Bj}, y_{Bj} are the real value of needle borders points while Δx_{Ai}, Δy_{Ai}, Δx_{Bj}, Δy_{Bj} are random errors. Hence, the coordinate of C_{ij} are $(x_{cij}+\Delta x_{cij}, y_{cij}+\Delta y_{cij})$, where $x_{cij}=\frac{x_{Ai}+x_{Bj}}{2}$, $y_{cij}=\frac{y_{Ai}+y_{Bj}}{2}$, $\Delta x_{cij}=\frac{\Delta x_{Ai}+\Delta x_{Bj}}{2}$, $\Delta y_{cij}=\frac{\Delta y_{Ai}+\Delta y_{Bj}}{2}$. The border errors only contain random errors without system errors because border points of each side are recovered by a group of HT lines.

Assume that $\Delta x_{Ai}, \Delta y_{Ai}, \Delta x_{Bj}, \Delta y_{Bj}$ are independent from each other and have the same distribution, with a mathematical expectation of zero and variance of σ^2 and that the final axis fitting by center points using the least square method is $y=\hat{a}_c x+\hat{b}_c$ while a_{real} is the real value of $\hat{a}_c$.

From all the assumption mentioned above, in the following part, we analyze the variance of $\hat{a}_c$ and $\hat{b}_c$. The variances reflect the accuracy of the measure parameter. The smaller the variance of the parameter is, the more accurate the measured parameter is. According to the least square method:

$$\hat{a}_c=\frac{\sum XY-\frac{1}{K}\sum X\cdot\sum Y}{\sum X^2-\frac{1}{K}(\sum X)^2} \tag{2}$$

$$\hat{b}_c=\overline{Y}-\hat{a}_c\cdot\overline{X} \tag{3}$$

Assume the number of center points (C_{ij}) used to fit an axis is K. So the value of K ranges from 2 to M×N. Substitute the coordinate of C_{ij} into Equation 2:

$$\hat{a}_c=\frac{a_{real}+\frac{1}{K\cdot{\sigma_{x_c}}^2}[\sum_{ij}(x_{cij}-\overline{x_c})\cdot\Delta y_{cij}+\sum_{ij}(y_{cij}-\overline{y_c})\cdot\Delta x_{cij}]}{1+\frac{2}{K\cdot{\sigma_{x_c}}^2}\cdot\sum_{ij}(x_{cij}-\overline{x_c})\cdot\Delta x_{cij}} \tag{4}$$

Where ${\sigma_{x_c}}^2$ and $\overline{x_c}$ represent the variance and mean value of x_{cij} respectively. Other symbols have similar meaning. According to Taylor expansion of Equation 4, we can get the following variance approximation (ignore high order terms):

$$D(\hat{a}_c)\approx\sum_{ij}\left(\frac{\partial\hat{a}_c}{\partial\Delta x_{cij}}\right)^2\Big|_{\substack{\forall i,j\\ \Delta x_{cij}=E(\Delta x_{cij})\\ \Delta y_{cij}=E(\Delta y_{cij})}}\cdot D(\Delta x_{cij})+\sum_{ij}\left(\frac{\partial\hat{a}_c}{\partial\Delta y_{cij}}\right)^2\Big|_{\substack{\forall i,j\\ \Delta x_{cij}=E(\Delta x_{cij})\\ \Delta y_{cij}=E(\Delta y_{cij})}}\cdot D(\Delta y_{cij})$$

$$=\frac{\sigma^2}{2K}\cdot\frac{(1+4{a_{real}}^2)\cdot{\sigma_{x_c}}^2+{\sigma_{y_c}}^2}{{\sigma_{x_c}}^4} \tag{5}$$

According to Equation 3, we can also get the variance of $\hat{b}_c$:

$$D(\hat{b}_c)\approx\frac{\sigma^2}{2K}\cdot[1+{a_{real}}^2+\frac{(1+4{a_{real}}^2)\cdot{\sigma_{x_c}}^2+{\sigma_{y_c}}^2}{{\sigma_{x_c}}^4}\cdot{\overline{x_c}}^2] \tag{6}$$

According to Equation 5 and 6, if K is large enough (K=MN for example), $D(\hat{a}_c)$ and $D(\hat{b}_c)$ will be small. Hence the accuracy will be improved by the created center points with large numbers.

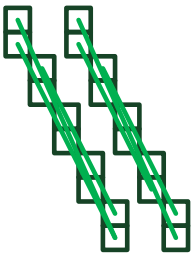

Fig. 9. Relationship between HT lines and edge points.

The relationship between HT lines and edge points is as shown in Fig. 9. The green lines are the HT lines along needle edge and the squares are the edge pixel points.

In [6], the two most external HT lines are used to compute an axis. In Fig. 9, as a matter of fact, each edge corresponds to multiple HT lines and these lines are not necessarily parallel with each other. For these reason, using two HT lines (one from left edge and one from right edge) to compute center line as needle axis is not accurate. By contrast, for the center point method, we do not utilize HT lines directly. Instead, we use HT lines to recover original edge points to eliminate multiple relationships in Fig. 9 and then create center points with large numbers. By fitting these large numbers of center points, the accurate needle axis can be obtained. From the analysis mentioned above, center point method is accurate than the method in [6].

For Equation 5, the approximation ignores the correlations among center points. For instance, C_{12} and C_{13} are related for both being created from the same point A_1. The larger K we choose, the stronger the correlations are. Although these correlations may influence accuracy, the results of experiments in section III also show that center point method is accurate than the method in [6].

III. Experimental Results

In this section, considering the fact that the robotic arm produced by KUKA Roboter GmbH has very high position and attitude precision, we use it to verify the accuracy of the needle's 3D orientation measured by binocular stereovision.

Fig. 10. Experimental environment.

Fig. 11. Surgical needle.

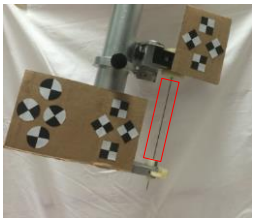

Fig. 12. Needle holder.

Fig. 10 shows our experimental environment. The whole system is combined with three parts: binocular stereovision system, laptop and robotic arm with surgical needle. As for binocular stereovision system, two Logitech webcams, with a resolution of 1280 ×720 pixels, are used. For laptop, the images are processed by MATLAB and camera calibration procedure is done by the Camera Calibration Toolbox in MATLAB. For robotic arm, it's the KUKA robotic arm with a pose repeatability accuracy of 0.03mm. The surgical needle (Fig. 11) is the real needle used in surgery, with a diameter of 1.22mm. The needle is fixed on the needle holder in Fig. 12. As shown in Fig. 12, we set a region of interest (inside the red line region) to use related algorithms to extract needle axis under a pure white background in the system calibration stage.

We move the robotic arm, at a low speed to ensure robotic arm's accuracy, to 37 different orientations, which are in different planes, and calculate the space angle between arbitrary two orientations in binocular stereovision system and robotic arm system respectively. Taking robotic arm system as the ground truth, the difference of these two calculation results is defined as the calculation error of needle orientation in binocular stereovision. This defined error can fully reflect the accuracy of the algorithm because this testing scheme eliminates the influence resulted from the system error of binocular stereovision system including its internal and external parameters' errors.

Assume the 3D orientation vector of the needle acquired by stereovision system is $\overrightarrow{n_I}$ (I=1,2,…,37) and by robotic arm system is $\overrightarrow{v_I}$ (I=1,2,…,37). We define that $\theta_{n_{I,J}}$ is the angle between $\overrightarrow{n_I}$ and $\overrightarrow{n_J}$ ($I \neq J$) while $\theta_{v_{I,J}}$ is the angle between $\overrightarrow{v_I}$ and $\overrightarrow{v_J}$ ($I \neq J$). For robotic arm's high accuracy, we take $\theta_{v_{I,J}}$ for ground truth. Although $\overrightarrow{n_I}$ and $\overrightarrow{v_J}$ cannot compare directly, $\theta_{n_{I,J}}$ and $\theta_{v_{I,J}}$ must be equal if no error exists. Orientation error can be characterized by $\theta_{n_{I,J}} - \theta_{v_{I,J}}$. In all, the orientation error is defined as follows:

$$\theta_{error_{I,J}} = \arccos\left(\frac{\overrightarrow{n_I}\cdot\overrightarrow{n_J}}{|\overrightarrow{n_I}|\cdot|\overrightarrow{n_J}|}\right) - \arccos\left(\frac{\overrightarrow{v_I}\cdot\overrightarrow{v_J}}{|\overrightarrow{v_I}|\cdot|\overrightarrow{v_J}|}\right) \quad (7)$$

TABLE I. ERROR COMPARISION

Method	Mean absolute value of error	Standard deviation of error	Max error
Method in [6]	0.9097°	0.8039°	4.2155°
Proposed Method	**0.3494°**	**0.2455°**	**0.9848°**

To compare the experimental results of these two methods (Hough lines method in [6] and the proposed center point method) for axis extraction, each method is applied to the same image data using the principle in Fig. 1 to calculate 3D orientation and the same criterion (Equation 7) to measure orientation error. In experiment, we choose parameter K=MN (max number) for center point method. For each method, we calculate $\{\theta_{error_{1,2}}, \theta_{error_{1,3}}, \ldots, \theta_{error_{36,37}}\}$, 666 ($C_{37}^2$) error data in total and calculate related statistics as Table Ⅰ shown.

According to the table, the proposed method improves the accuracy of needle orientation determination, by approximately 70% compared to previous related work. This result is consistent with analysis in section Ⅱ-B.

IV. CONCLUSION

In this paper, a new method for needle axis extraction is introduced. The method makes full use of edge points from two sides of the needle and creates center points through which an accurate axis is extracted. It has been proved experimentally to be more accurate than previous method. The proposed method improves the accuracy of needle orientation determination, by approximately 70% compared to previous related work.

REFERENCES

[1] B. Treepong, N. Tanaiutchawoot, C. Wiratkapun and J. Suthakorn, "On the design and development of a breast biopsy navigation system: path generation algorithm and system with its GUI evaluation," Biomedical and Health Informatics (BHI), 2014 IEEE-EMBS International Conference on. IEEE, 2014.

[2] G. J. Bootsma, J. H. Siewerdsen, M. J. Daly and D. A. Jaffray, "Initial investigation of an automatic registration algorithm for surgical navigation," Engineering in Medicine and Biology Society, 2008. EMBS 2008.

[3] G. Zheng, L. Gu, X. Li and J. Zhang, "Computer-assisted preoperative planning and surgical navigation system in dental implantology," Information Technology Applications in Biomedicine, 2007. ITAB 2007.

[4] R. Yang, Z. Wang, S. Liu and X. Wu, "Design of an Accurate Near Infrared Optical Tracking System in Surgical Navigation," Journal of Lightwave Technology, vol.31, no.2, pp.223-231, Jan.15, 2013.

[5] S. A. Nicolau, L. Goffin, and L. Soler, "A low cost and accurate guidance system for laparoscopic surgery: Validation on an abdominal phantom," Proceedings of the ACM symposium on Virtual reality software and technology. ACM, pp.124-133, 2005.

[6] L. Goffin, G. Bour, F. Martel, S. Nicolau, J. Gangloff, J.M. Egly and B. Bayle, "Design and In Vivo Evaluation of a Robotized Needle Insertion System for Small Animals," IEEE Trans. Biomedical Engineering, vol.60, no.8, pp.2193-2204, Aug 2013.

[7] A. Ayadi, B. Bayle, P. Graebling and J. Gangloff, "An image-guided robot for needle insertion in small animal. Accurate needle positioning using visual servoing," IEEE/RSJ International Conference on Intelligent Robots and Systems (IROS), pp.1453-1458, 22-26 Sept. 2008.

[8] J. S. Hong, T. Dohi, M. Hasizume, K. Konishi and N. Hata, "A motion adaptable needle placement instrument based on tumor specific ultrasonic image segmentation," Medical Image Computing and Computer-Assisted Intervention—MICCAI 2002, Springer Berlin Heidelberg, pp. 122-129, 2002.

[9] N. Garcia-Morales, D. Lorias, V. Gonzales and F. Chico, "Development of an Algorithm for Register the Movement of the Instrumental in a Simulator for Screw Positioning in the Lumbar Region," 2014 IEEE 27th International Symposium on Computer-Based Medical Systems (CBMS), pp.109-112, 27-29 May 2014.

[10] H. Zhou, W. Qiu, M. Ding, S. Zhang, "Automatic needle segmentation in 3D ultrasound images using 3D improved Hough transform," Medical Imaging, International Society for Optics and Photonics, pp. 691821-691821, 2008.

[11] R. Jain, R. Kasturi and B. Schunck, Machine Vision, McGraw-Hill,New York, 1995.